Ion-beam induced oxidation of GaAs and AlGaAs

J. L. Alay
IMEC, Kapeldreef 75, B-3001 Leuven, Belgium and LCMM, Facultat de Física, Universitat de Barcelona, Diagonal 645, E-08028 Barcelona, Catalonia, Spain

W. Vandervorst and H. Bender
IMEC, Kapeldreef 75, B-3001, Leuven, Belgium

The oxidation of GaAs and $Al_xGa_{1-x}As$ targets by oxygen irradiation has been studied in detail. It was found that the oxidation process is characterized by the strong preferential oxidation of Al as compared to Ga, and of Ga as compared to As. This experimental observation, which has been accurately quantified by using x-ray photoelectron spectroscopy, is connected to the different heats of formation of the corresponding oxides. The oxide grown by ion-beam oxidation shows a strong depletion in As and relatively low oxidation of As as well. The depletion can be associated with the preferential sputtering of the As oxide in respect to other compounds whereas the low oxidation is due to the low heat of formation. In contrast Al is rapidly and fully oxidized, turning the outermost layer of the altered layer to a single Al_2O_3 overlayer, as observed by transmission electron microscopy. The radiation enhanced diffusion of oxygen and aluminum in the altered layer explains the large thickness of these altered layers and the formation of Al oxides on top of the layers. For the case of ion-beam oxidation of GaAs a simulation program has been developed which describes adequately the various growth mechanisms experimentally observed. © 1995 American Institute of Physics.

I. INTRODUCTION

A detailed understanding of the fundamentals of secondary ion mass spectrometry (SIMS) analysis can only be obtained by a thorough evaluation of the ion-solid interaction. In the particular case of concern here, i.e., dynamic SIMS, oxygen is a frequently used ion beam. Hence the processes occurring during oxygen irradiation deserve a detailed study.

Moreover oxygen bombardment of materials constitutes also a new method to grow oxides which are otherwise not so easily formed with conventional thermal processes. Previous studies on ion-beam oxidation of Si have indeed shown the possibility to grow oxides by ion bombardment.[1-4] With respect to the modeling of the growth process it has been shown that a simple ion retention model[5] during sputtering as previously proposed is inadequate in describing all the effects occurring and other dynamic aspects such as compound formation need to be considered as well.

The present investigation is focused on the ion-beam induced oxidation of GaAs, $Al_{0.4}Ga_{0.6}As$, and $Al_{0.8}Ga_{0.2}As$ targets during O_2^+ bombardment, as occurring during SIMS analysis. In this respect we have performed a study of the surface stoichiometry of the grown oxides, the dynamics of the oxide growth, and the stoichiometry of the underlying layers.

Compared to the ion-beam oxidation of Si, the situation of III-V semiconductor materials is much more complex since one has now not only to consider the degree of oxidation but also eventual preferential removal or oxidation of one of the constituents of these targets. For instance, it is widely known that the Al of $Al_xGa_{1-x}As$ shows a very strong oxidation after exposure to the atmosphere, an effect which could be persistent during ion-beam oxidation.

Previous work on ion-beam oxidation of GaAs has indicated that Ga is preferentially oxidized with respect to As and that the degree of preferential oxidation is strongly energy dependent.[2,4,6] No previous results on the ion-beam oxidation of $Al_xGa_{1-x}As$ targets have been reported.

Some introductory work, using *in situ* x-ray photoelectron spectroscopy (XPS), regarding the oxidation of GaAs and $Al_{0.8}Ga_{0.2}As$ has already been reported in Refs. 7 and 8.

In the first part of this article we present an overview of the experimental characterization of the ion-beam induced oxidized $Al_xGa_{1-x}As$ targets (x=0.0, 0.4, and 0.8) with respect to the altered layer stoichiometry and the oxygen incorporation, measured by XPS, and a complete study on the structure of the build-up oxides by high-resolution transmission electron microscopy (HREM).

In order to understand the experimental results a simulation program Chemical-ISRD (CISRD), which is based on the reported ISRD code,[4,9] has been developed. Whereas the latter was intended to simulate the ion-beam induced oxidation of Si targets, the new CISRD code presented in this work is capable of simulating the different physical mechanisms operative during the ion bombardment of the GaAs targets. This program and the results obtained with it will be described in the second part of this article.

II. EXPERIMENT

The ion-beam oxidation of III-V semiconductor materials was performed on three different compounds: GaAs, $Al_{0.4}Ga_{0.6}As$, and $Al_{0.8}Ga_{0.2}As$. For the first case a 3 in. GaAs (100) wafer was used. The ternary compounds have been grown by molecular beam epitaxy (MBE) on a 3 in. GaAs (100) wafer: 2.2 μm of $Al_{0.4}Ga_{0.6}As$ on a 0.7 μm GaAs buffer and 1.1 μm of $Al_{0.8}Ga_{0.2}As$ on 0.7 μm GaAs buffer.

0021-8979/95/77(7)/3010/13/$6.00

None of the samples was chemically treated prior to the ion-beam bombardments, and samples in the shape of small cleaved pieces were loaded inside the analysis chamber of the XPS instrument where the ion bombardment takes place. The Al concentration in the $Al_xGa_{1-x}As$ samples has been determined by wavelength dispersive spectroscopy. From this analysis an x of 0.88 was found for the aimed 0.80 compound and an x value of 0.43 for the 0.40 intended compound.

The samples have been bombarded with an O_2^+ ion beam with energies between 1 and 5 keV, at different angles of incidence, ranging from 0° to 60° (referred to the target normal), while rastering over 4×4 mm^2 or 2×2 mm^2. In situ XPS data, using a SSX-100 instrument (monochromatic Al $K\alpha$ radiation with a 300 μm spot size) were taken from the center of the rastered area once the steady state was reached. For some cases like 5 keV at normal incidence, the evolution of the surface stoichiometry was measured as a function of bombardment time until the steady state was reached. The base pressure of the analysis chamber is in the 10^{-10} Torr range and rises to 10^{-8} Torr range during oxygen bombardment.

The surface chemical composition, as analyzed by XPS, is based on the Ga 3d, As 3d, Al 2p, and O 1s photoelectron peaks.[10–12] The attenuation length of the photoelectrons has been calculated for GaAs and the various $Al_xGa_{1-x}As$ matrixes.[13] The matrix effect is found to be negligible, and therefore attenuation length calculations are limited to the GaAs-matrix case because of its simplicity.

Based on the above identification of the various states, a deconvolution of the photoelectron peak is performed to determine from the respective peaks, the absolute concentration of each chemical state (at. %) and the relative fraction of it in the total photoelectron peak (rel%) within the sampling volume. For example, the relative fraction of oxidation or relative oxidation (rel%) of As, gives the amount of As turned into As oxide relative to the total amount of As measured.

A HREM study of a [110] cross section of the altered layer formed by a 5 keV O_2^+ ion beam with normal incidence on all targets has been carried out. The [110] cross-section specimens are prepared by grinding and dimpling, and subsequently ion milling as outlined in Ref. 14. HREM examinations are performed on a JEM 4000 EX (400 kV).

III. RESULTS

A. XPS

The influence of the ion energy, the angle of incidence, and the Al content (x) on the ion-beam induced oxidation of the $Al_xGa_{1-x}As$ targets is summarized in Figs. 1–3.

In Fig. 1 the evolution of the relative oxidation for Al, Ga, and As is shown as a function of the Al content for normal incidence bombardments with ion energies of 1 and 5 keV. In the 1 keV case the degree of oxidation is very high and remains nearly constant for all species with increasing Al content. In the 5 keV case, the evolution of the Al and Ga degree of oxidation does not differ significantly from the low energy one, but the As oxidation is strongly favored by the presence of Al atoms.
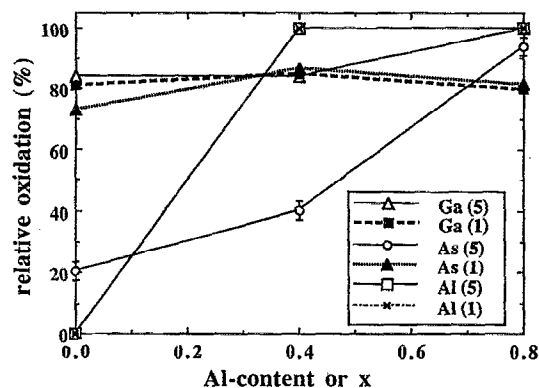

FIG. 1. Dependence of the Al, Ga, and As relative oxidation on the Al content for 1 keV (dashed line) and 5 keV (solid line) O_2^+ normal incidence bombardments. Note that the Al data coincide for both energies.

The incorporation of oxygen in the surface of the altered layer is shown in Fig. 2 as a function of the angle of incidence for the 1 and 5 keV cases. For the 1 keV bombardments a small decrease of the amount of incorporated oxygen can be observed with increasing angle of incidence. For the 5 keV bombardments only the incorporation of oxygen in GaAs targets exhibits a strong reduction with increasing angle of incidence, but again, this dependence for the oxygen content comes accompanied by an increase in arsenic content with increasing angle of incidence. Since the increase coincides with a decrease in the arsenic degree of oxidation, the arsenic replacement by oxygen atoms is seen as a consequence of the chemical preferential sputtering on As-oxide molecules. Finally in Fig. 3, the dependence for the degree of oxidation and the incorporation of oxygen as a function of the ion-beam energy (normal incidence) is shown. The As relative fraction of oxidation is clearly the only quantity influenced by the ion energy, whereas the Al content, at high concentrations $x=0.8$, seems to act as a chemical catalyst for the As oxidation as well.
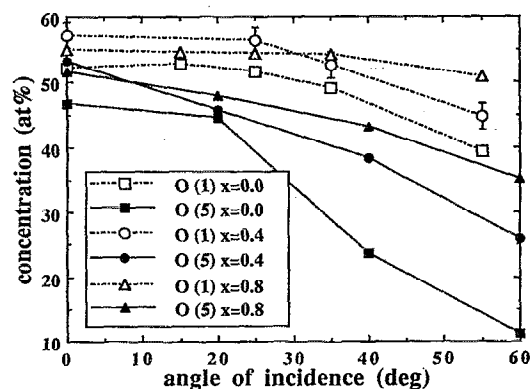

FIG. 2. Total O concentration as a function of the angle of incidence for 1 and 5 keV energies for various $Al_xGa_{1-x}As$ substrates.

J. Appl. Phys., Vol. 77, No. 7, 1 April 1995
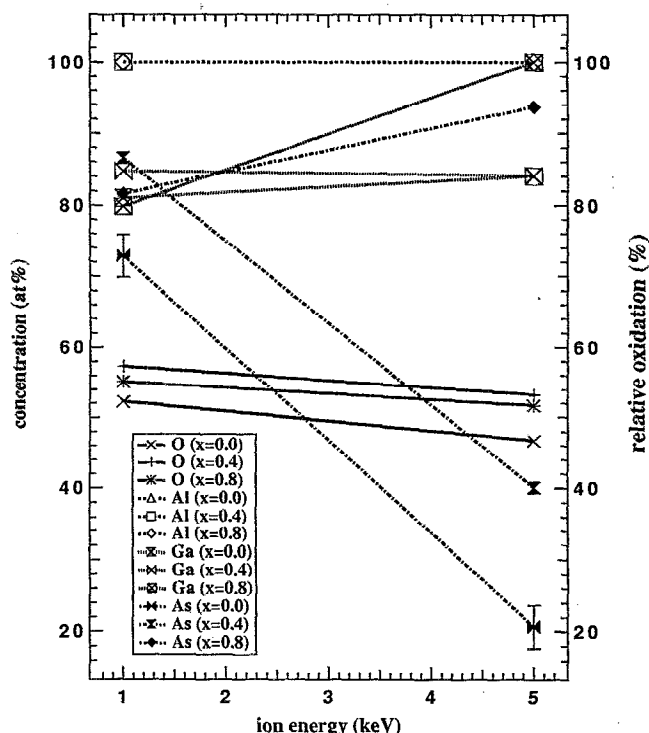
Alay, Vandervorst, and Bender   3011

FIG. 3. Relative oxidation (referred to the right-hand axis) of Al (dashed line), Ga (dotted line), As (dotted-dashed line) and total amount of O (solid line, referred to the left-hand axis) of $Al_xGa_{1-x}As$ as a function of the ion energy (lines are drawn to guide the eye).

B. HREM

1. Results for GaAs

Figure 4(a) shows the HREM picture of the oxide formed on GaAs (5 keV, normal incidence). The altered layer clearly consists of a uniform amorphous layer in the surface region, without the presence of any sizable microcrystalline regions. This layer can be identified as an amorphous (oxide) layer based on the contrast with the underlying crystalline GaAs. The surface of the oxide layer retains a flat profile over a very long range. A rather sharp interface separates the oxide layer from the GaAs lattice, although the altered layer continues beneath this "chemical" interface. The (100) GaAs lattice can be well resolved, although the presence of dark regions, reveal the formation of damage well beyond the mean projected range of the implanted oxygen ions. From the knowledge of the lattice parameter of GaAs (0.5653 nm) the HREM micrograph has been accurately calibrated, and therefore the structure of the altered layer can be accurately analyzed.

The oxide layer is 14.1 nm thick, while the interface region never extends larger beyond 1.1 nm. The better contrast, obtained in the low magnification picture shown in Fig. 5, reveals the extent of the altered layer composed of the oxide layer and a damaged region. The thickness of the latter is 10.1 nm and consequently the total thickness of the altered layer approaches about 24.2 nm, which is far beyond the mean penetration depth of 5 keV O_2^+ ions. TRIM (Transport of Ions in Matter)[15-17] simulations indicate that such a mean
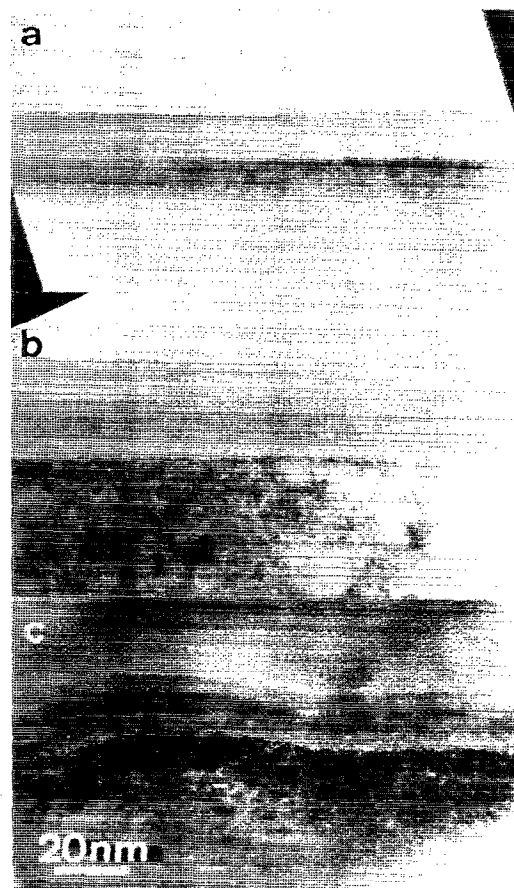

FIG. 4. TEM [110] cross sections of the GaAs (a), $Al_{0.4}Ga_{0.6}As$ (b), and $Al_{0.8}Ga_{0.2}As$, (c) targets after a 5 keV O_2^+ bombardment at normal incidence.

projected range comparable to the thickness of the oxide layer would require a 12 keV O_2^+ ion beam normally incident on the surface. Clearly then, additional physical mechanisms, unaccounted for in the TRIM code, are needed to explain the thickness of the oxide layer.

2. Results for $Al_{0.4}Ga_{0.6}As$

Figure 4(b) shows the HREM picture for $Al_{0.4}Ga_{0.6}As$. Again one can observe a similar two-layer structure as in the case of GaAs. The first layer is completely amorphous and

FIG. 5. HREM [110] cross section of GaAs after a 5 keV O_2^+ bombardment at normal incidence.
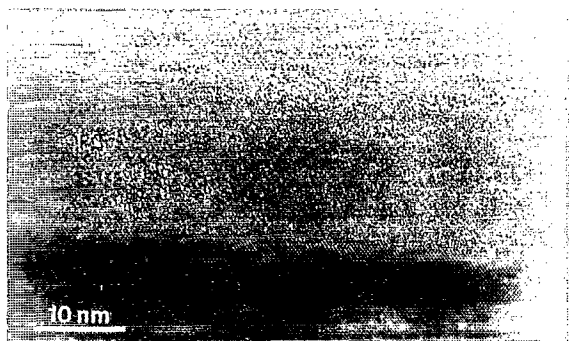
Alay, Vandervorst, and Bender

FIG. 6. HREM [110] cross section of $Al_{0.4}Ga_{0.6}As$ after a 5 keV O_2^+ bombardment at normal incidence.
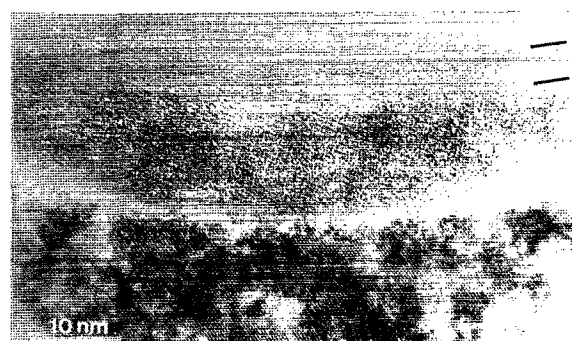

FIG. 7. HREM [110] cross section of $Al_{0.8}Ga_{0.2}As$ after a 5 keV O_2^+ bombardment at normal incidence.

corresponds to the built-up oxide. The altered layer extends beneath the oxide as a damaged layer retaining crystalline properties. The latter is separated from the oxide layer by a sharp interface.

But the most striking feature in this transmission electron microscopy (TEM) picture is the presence of a layer structure in the oxide layer itself. Near the top surface, we now observe an amorphous oxide layer with brighter contrast, indicating that lighter (in atomic mass) species are present in this layer than in the underlying thicker oxide. This can be interpreted as a layer enriched in Al oxide, while the underlying thicker oxide contains more of the heavier compounds like Ga oxide and As oxide. These results suggest that a strong aluminum diffusion mechanism plays a major role in the process of formation of the oxides, as will be described in Sec. IV.

The top surface is not perfectly flat, but a certain roughness can be observed (Fig. 6). The roughness, however, originates from the MBE growth process and has no relation to the ion-beam induced oxidation. The appearance of surface roughness in the $Al_xGa_{1-x}As$ layers during the MBE growth is highly dependent on the temperature of deposition and increases with the aluminum content. This effect will be addressed later.

By using the interatomic distance as a ruler, we find a thickness of 16.9 nm for the total oxide layer comprising a top oxide layer of 4.2 nm and a thick oxide of 12.7 nm, whereas the damaged layer, observed in picture 4(b), has a thickness of 13.1 nm. The thickness of the interface between the oxide and the damaged layer is less than 1 nm. This results in a 30.0-nm-thick altered layer, again far beyond the mean projected range of the O_2^+ ion beam. The TRIM code indicates that an energy of more than 12 keV would be required to reach a mean projected range of 16.9 nm. Again, this points towards the presence of some additional mechanisms for oxide layer formation, beyond the simple retention model and not taken into account in the TRIM simulations.

3. Results for $Al_{0.8}Ga_{0.2}As$

Figure 4(c) shows the HREM picture for $Al_{0.8}Ga_{0.2}As$. Again one observes an amorphous oxide layer and an underlying damage layer, separated by a sharp interface. The oxide layer itself again has a two-layer structure with a thin aluminum oxide-enriched layer on top and a layer beneath containing heavier species, namely gallium and arsenic oxide. The larger contrast in the micrograph between both oxide layers suggests an enhanced aluminum content in the top layer as compared to the layer formed on $Al_{0.4}Ga_{0.6}As$. Important, however, is that neither the top oxide nor the thicker oxide contain any sizable microcrystalline regions. A mechanism involving a strong driving force for the aluminum diffusion towards the surface must be operative during the buildup of the oxide layer to explain the formation of such an overlayer. The damaged layer present beneath the oxide retains a crystalline structure. In Fig. 7 the entire altered layer, composed of the oxide and the damaged layer, is shown, where the latter presents the darkest contrast.

The thin oxide overlayer is 5.6 nm, and the underlying oxide is 12.7 nm thick, resulting in a total oxide thickness of 18.3 nm. The interface thickness is smaller than 1.0 nm. The damaged layer is 15.4 nm thick, so the entire altered layer reaches a thickness of 33.7 nm, being even thicker than the one observed on $Al_{0.4}Ga_{0.6}As$ and GaAs. The TRIM code would require energies of 15 keV to reach this large penetration range.

An increase in long range surface roughness is observed in Fig. 8, similar to the $Al_{0.4}Ga_{0.6}As$ case, corresponding to a roughness wavelength of 245 nm. This roughness wavelength originates from the MBE growth and is not the result of the ion-beam bombardment, since the formation of rippled surfaces in Si, GaAs, and $Al_xGa_{1-x}As$ targets by the ion-beam bombardment itself is observed only far from normal incidence (30°–60°). In order to confirm the origin of the

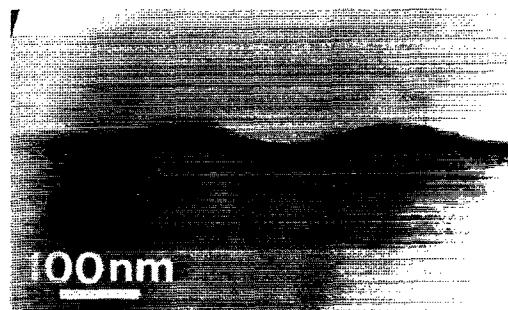FIG. 8. TEM [110] cross section of $Al_{0.8}Ga_{0.2}As$ after a 5 keV O_2^+ bombardment at normal incidence.

J. Appl. Phys., Vol. 77, No. 7, 1 April 1995

Alay, Vandervorst, and Bender   3013
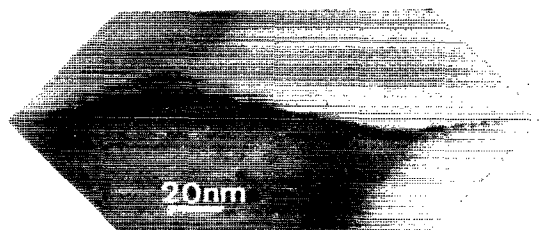
FIG. 9. TEM [110] cross section of $Al_{0.8}Ga_{0.2}As$ before bombarding.

observed roughness, Figs. 9 and 10 show two micrographs of the target before any bombardment was performed. The same roughness characterized by the same wavelength found after the oxygen bombardment is observed, although the latter tends to smooth the roughness. The irregular native oxide covers the surface and has a mean thickness of 1.7 nm.

IV. SIMULATION CODE

The interpretation of the experimental results is not directly straightforward. Schultz and Wittmaack have proposed a model for the ion retention during sputtering,[5] which in stationary state gives a value for the surface concentration of the implanted species inversely proportional to the sputter yield. As already shown for the case of the oxygen bombardment of Si, the model ignores any thermodynamic effects and predicts unrealistically high values of oxygen. The latter is particularly true when the calculated value of the surface concentration exceeds the concentration of stable oxides like SiO_2. On the other hand the model is adequate when predicting the angular dependence of the oxygen concentration in Si, as soon as the sputter yield becomes large enough such that the calculated value was lower than the SiO_2 limit. A problem which was observed in addition, is that the thickness of the grown oxide is larger than the one calculated based on range statistics. The larger thickness could be explained by invoking additional oxygen diffusion.

Again for the case of III-V compounds one could try to apply the simple model of Schultz and Wittmaack. The results shown in Fig. 2 with respect to the angular dependence indicate however the inadequacy of the model. If it were applicable the oxygen concentration should follow the angular dependence of the sputter yield which is roughly $1/\cos\theta$, where θ is the angle of incidence. As can be seen in Fig. 3
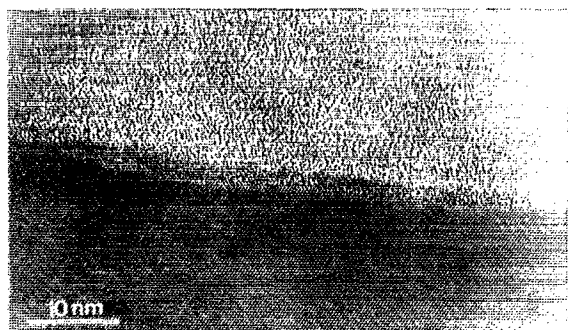

FIG. 10. HREM [110] cross section of $Al_{0.8}Ga_{0.2}As$ before bombarding.

the oxygen concentration hardly changes when going from $0°$ to $60°$ and is hence far from the predicted $1/\cos\theta$ dependence. Moreover the model ignores completely any effects due to preferential oxidation (cf. Fig. 1) and preferential sputtering (cf. Fig. 3). Therefore a more refined treatment is required. For the case of Si, a simulation code has been developed which in addition to simple ion retention and sputtering effects, incorporates oxygen diffusion and desorption.[4,9] By combining those mechanisms it has been possible to predict the growth of oxides on Si accurately. One is therefore tempted to adapt the program to the oxygen bombardment of III-V materials as well.

In view of the complexity of the program, we will restrict ourselves in this article to the simulation of the oxygen bombardment of GaAs. Further extension to $Al_xGa_{1-x}As$ is equally possible but is far more complicated by the strong Al diffusion causing the formation of the double layer structure in the oxide.

The CISRD code is based on the concepts introduced by Vancauwenberghe et al. in their ISRD program.[4,9] Basically this program describes the interaction of the oxygen beam with the target as follows. The bombardment of the target is considered in small incremental doses. For each dose the incorporation statistics of the primary ion, the sputtering of the target, and the implanted atoms are calculated using dynamic TRIM. Following this calculation a set of equations is solved, which describes the reaction between free oxygen and the target constituents as well as the diffusion of the free oxygen. The diffusion constant itself is depth dependent and determined by the defects produced (calculated by TRIM) by the incident ions. Surface desorption of free oxygen is considered as well. After this calculation, the target composition is updated and the whole process is started again.

The extension of this program from Si to GaAs requires the extension of the equations now describing the formation of Ga and As oxides (instead of only Si oxides) as well as the sputtering of Ga and As atoms from GaAs, and the Ga and As oxides. Note that each rate equation has its own reaction constant which implies that preferential oxidation can be introduced.

The CISRD model was implemented for the case of O_2^+ ion bombardment of GaAs at normal incidence. This simulation code requires the determination of three sets of parameters for each of the species (Ga and As) and each compound (GaAs, Ga_2O_3, and As_2O_3) since the model distinguishes between target atoms involved in oxide and metallic bonds. Some of the parameters can be derived from empirical data, while some of them are totally unknown.

In conclusion, the starting situation is as follows.
(a) Interaction ion–solid[18]

(i) Determined *a priori*: (1) Binding energy of elemental Ga: 2 eV (semiconductor); (2) Binding energy of elemental As: 2 eV (semiconductor); (3) Surface binding energy of elemental Ga: 0.63 eV (obtained by subtracting the binding energy from the sublimation energy which is 2.63 eV for GaAs); and (4) Surface binding energy of elemental As: 0.63 [as for case (3)].

Alay, Vandervorst, and Bender

(ii)   To be determined: Binding energies and surface bind-
ing energies for the oxidized species.

(b) Diffusion

Determined *a priori*: The values[4] used for the case of oxygen
bombardment of Si were chosen for the GaAs as well, i.e., a
thermal diffusion constant of 1×10^{-14} cm^2/s and radiation-
enhanced diffusion constant of 1×10^{-12} cm^2/s. The choice
of these values is not completely free since the selection of
lower values (by one order of magnitude) for the radiation-
enhanced diffusion coefficients gives rise to an unrealistic
accumulation of free oxygen concentrations in the altered
layer of about 1×10^{24} at/cm^3, because now the oxygen dif-
fusion is too slow such that the free oxygen cannot reach the
surface and desorb. Therefore, the radiation-enhanced diffu-
sion coefficient in the oxide layer must be of the same order
of magnitude as the one in the case of silicon oxide layers.
With respect to the thermal diffusion coefficient (D), its
value is only relevant at very low energies (<1 keV),
whereas at higher energies it plays only a minor role in the
determination of the total oxide thickness. In fact the calcu-
lated oxide thickness only varies with 1 nm whether the ther-
mal diffusion is included ($D = 1 \times 10^{-14}$ cm^2/s) or not ($D = 0$
cm^2/s). Using the former value, the simulated thicknesses
approach better the experimental results derived from the
TEM pictures.

(c) Reaction constants:

(i)   To be determined: the reaction rate constants for gal-
lium and arsenic (K_{gaox} and K_{asox}).

The actual procedure used to determine the unknown
parameters is based on an iterative procedure, whereby we
choose the parameters such that the results for 1 and 5 keV,
normal incidence, bombardments on GaAs are correctly pre-
dicted simultaneously. Note that not only the stoichiometry
needs to be predicted, but also the degree of oxidation of the
individual components, as well as the sputter yields, the time
profiles, and the thickness of the altered layer.

In order to compare the simulations with the experimen-
tal data, one must take into account the finite sampling depth
of the XPS experiments, and therefore calculate starting from
the simulated concentration profiles, the theoretical XPS
concentrations, taking into account the effect of the electron
escape depth.

The XPS atomic concentration of a specific target ele-
ment (C_i) is the Laplace transform of the element profile
within the target ($L[c_i(x)]$). The Laplace transform of the
concentration function is defined as

$$L[c_i(x)] = \int_0^\infty c_i(x)\exp(-xp)dx = C_i(p).$$

By introducing the variable $p = 1/\lambda \sin \varphi$, where λ is the at-
tenuation length of the photoelectrons emitted at each depth
and φ is the take-off angle (in the case of our measurements
fixed at 35°), the respective XPS atomic concentrations C_i
for i=Ga, As, and O are defined.

In Fig. 11 the dependence of the exponential factor of
the Laplace transform is shown for each of the target ele-
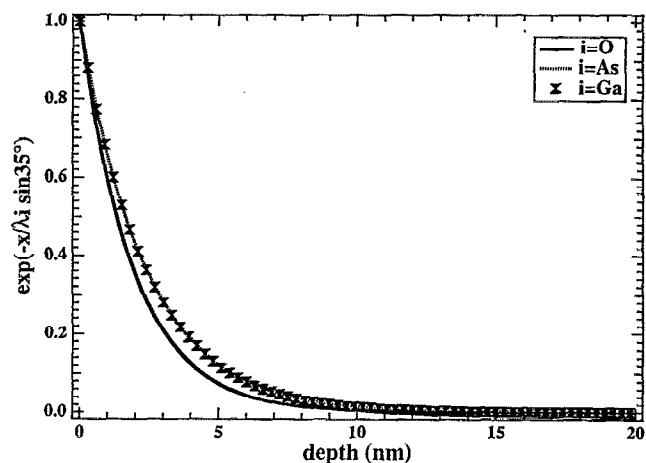ments (Ga, As, and O). This function is derived using the

FIG. 11. Exponential factor in the Laplace transform for O and each of the
target elements in GaAs.

corresponding attenuation length[14] (λ_{Ga}=4.1 nm, λ_{As}=4.1
nm, λ_O=3.3 nm). As could be expected from the values of
the attenuation lengths, which are strongly energy dependent,
the signal measured by XPS corresponding to Ga and As
originates from approximately the same depth, whereas the
O signal arises from layers closer to the surface. We recall
that the variation in attenuation lengths results from the dif-
ference in kinetic energies, i.e., lower kinetic energy of O
[E_k(O $1s$)=957 eV] as compared to Ga [E_k(Ga $3d$)=1467
eV] and As [E_k(As $3d$)=1444 eV].

In order to compare the simulated data with the XPS
results, the CISRD concentration profiles were Laplace trans-
formed leading to the quantities C_{Ga}^{XPS}, C_{As}^{XPS}, and C_O^{XPS}. Part
of the iteration then includes a redefinition of the parameters
used in the simulation (binding energy, surface binding en-
ergy, and reaction constant), trying to fit the corresponding
concentrations at that energy. The process is repeated until
the CISRD code results in satisfying simulations of the XPS
experimental concentrations for both the 1 and 5 keV energy.
A supplementary constraint that must be satisfied is that the
value of the GaAs sputter yield at 5 keV should coincide
with the experimental 0.85 atoms/O-atom.

The collection of parameters which were found to fulfill
the above mentioned requirements are:

(a)   Interaction ion-solid: (1) Binding energy of Ga in ox-
ide: 1.00 eV; (2) Binding energy of As in oxide: 1.00
eV; (3) Surface binding energy of Ga in Ga$_2$O$_3$: 0.40
eV; and (4) Surface binding energy of As in As$_2$O$_3$:
0.10 eV.
(b)   Chemical reaction: (1) 1 keV O$_2^+$ bombardment:
$K_{Ga_2O_3} = 6.67 \times 10^{-20}$ cm^3/s and $K_{As_2O_3} = 0.17$
$\times 10^{-20}$ cm^3/s; and (2) 5 keV O$_2^+$ bombardment:
$K_{Ga_2O_3} = 0.67 \times 10^{-20}$ cm^3/s and $K_{As_2O_3} = 0.02$
$\times 10^{-20}$ cm^3/s.

A. Significance of the CISRD parameters for GaAs

All the ion-solid interaction parameters derived for the
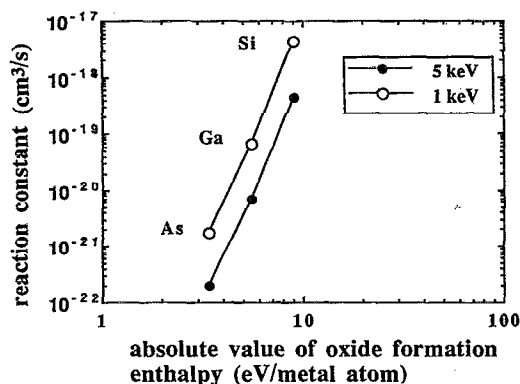oxides indicate a strong tendency towards preferential sput-

FIG. 12. Reaction constant as a function of the heat of formation of the oxide (SiO$_2$, Ga$_2$O$_3$, and As$_2$O$_3$) for 1 and 5 keV ion-beam energies.

tering of the oxide phases, since the surface binding energy, binding energy, and consequently the sublimation energy for these compounds are rather low as compared to the metallic phases. This is especially important for the arsenic oxide, since the derived surface binding energy (SBE) is quite small [SBE(Ga$_2$O$_3$)=4SBE(As$_2$O$_3$)], a fact corroborating the mechanism of chemical preferential sputtering of As$_2$O$_3$, which was already pointed out in the XPS section. This reduced value of the surface binding energies for the oxidized phases makes it more difficult to form oxides by O$_2^+$ ion-beam bombardment of GaAs targets. This difficulty does not exist in the case of silicon targets because of the rather large value for the surface binding energy of silicon oxide [SBE(SiO$_2$)=1.95 eV].[4]

The reaction constants present a more complicated behavior. For a 5 keV O$_2^+$ bombardment, the $K_{As_2O_3}$ is found to be 40 times smaller than $K_{Ga_2O_3}$, a relation which seems to support the strong preferential oxidation of gallium with respect to arsenic, as previously observed in all XPS measurements. If we compare $K_{Ga_2O_3}$ with the value obtained for Si at the same energy of bombardment, we find that K_{SiO_2} is 66 times larger than $K_{Ga_2O_3}$, reflecting the strong oxidation tendency of Si as compared to the other elements (Ga and As). The large difference in reaction constants between the different species suggests the existence of a strong dependence of K on a thermodynamic quantity accounting for the tendency of the species to become oxidized. The thermodynamic magnitude which gives a quantitative and qualitative measure of the energetic balance for a chemical reaction is the heat of formation of a compound. The heat of formations[19] of SiO$_2$, Ga$_2$O$_3$, and As$_2$O$_3$ are -8.78 eV/metal atom, -5.54 eV/metal atom, and -3.38 eV/metal atom, respectively, showing the decreasing tendency to oxidize, which correlates with a decrease in reaction constant. Figure 12 suggests an exponential dependence of the reaction constant on the heat of formation of the oxide. Another remarkable property for the reaction constant is its dependence on the ion-beam energy, whereby the reaction constant for the target species during a 1 keV bombardment exceeds the one for 5 keV bombardment by more than one order of magnitude. This effect is

very important in the case of arsenic, since due to the very small value of its reaction constant at 5 keV, only a small increase of it implies a considerable increment in the formation of As$_2$O$_3$. Such an increase does not represent any significant variation in the Si and Ga oxidation level because of the already large reaction constant for 5 keV impingement.

Although the experiments were performed at room temperature in the analysis chamber of the XPS instrument, the penetration depth of energetic ion beams gives rise to thermal spike effects in the target matrix. These should be taken into account when considering very critical oxidation processes, such as the arsenic oxidation.

As was described by Kelly et al.[20,21] prompt thermal processes consisting of brief temperature excursions take place during the bombardment of the target. The temperature transient caused by the incoming ions is expressed by

$$\Delta T \approx E_i / \Delta x \Delta y^2 N 3k,$$

where E_i is the energy of the incoming ion, Δx is the mean x straggling of the damage, Δy is the mean y straggling of the damage, N is the number density of the target, and $3k$ is the assumed heat capacity per atom. By using this expression we can calculate the bombardment energy leading to the highest prompt temperature excursion

$$\frac{\Delta T(1 \text{keV})}{\Delta T(5 \text{keV})} = \frac{1 \Delta x(5 \text{keV}) \Delta y^2 (5 \text{keV})}{5 \Delta x(1 \text{keV}) \Delta y^2 (1 \text{keV})}.$$

If we substitute the values of the mean x and y stragglings by those obtained using the TRIM code, the following relations are obtained:

$$\Delta T(1 \text{keV}) = 4.2 \Delta T(5 \text{keV}) \quad \text{for a GaAs target,}$$

$$\Delta T(1 \text{keV}) = 4.5 \Delta T(5 \text{keV}) \quad \text{for a Si target.}$$

These indicate that the maximum temperature reached by the lattice due to the ion bombardment is approximately four times higher for a low energy bombardment of 1 keV than for a higher energy bombardment of 5 keV. This is mainly due to the size of the interaction volume. The latter is much smaller for low energies than for high energies, and hence the density of deposited energy by the incoming ion is larger at low energies. The higher local temperature increase of the lattice favors the chemical reaction of oxygen with the target atoms at low ion energies, and therefore leads to different reaction constants for different energies of bombardment. In order to fit the 1 and 5 keV data for GaAs, the reaction constant for As needs to be increased with one order of magnitude for the 1 keV bombardment. From this fitting and assuming that this change is proportional with the different temperatures in the thermal spikes, we can calculate what the reaction constant for Ga would be. In the case of Si, a similar proportionality is assumed. Within this concept one then arrives at two different curves, each corresponding to a different ion energy, describing the reaction constant as a function of the enthalpy of formation (cf. Fig. 12). This result is especially important in the case of As oxidation which, for a 5 keV O$_2^+$ bombardment, has a very low reaction constant due to its low oxide heat of formation. The reaction constant for arsenic oxide is ten times higher for a 1 keV bombardment, a
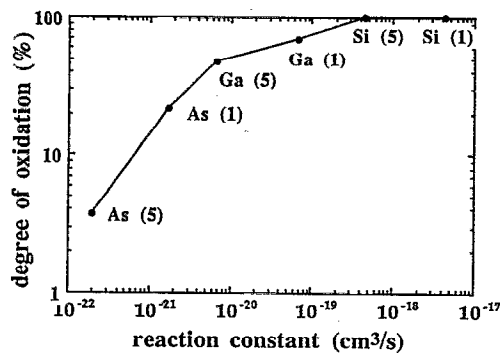
FIG. 13. Mean degree of oxidation of the altered layer for GaAs and Si as a function of the reaction constant.

FIG. 14. Steady state internal profile of GaAs target after a 1 keV O_2^+ bombardment at normal incidence, simulated using the CISRD model. The depth scale is measured with respect to the original surface, whereas the instantaneous surface is located at the depth of 8.4 nm.

fact which accounts for the prompt thermal excursion effect. This high reaction constant will strongly increase the oxidation in agreement with the experimental XPS observations. The increase of the reaction constant for gallium oxide by the same factor does not play a determining role, since the reaction constant at 5 keV is already large, and therefore the oxidation of gallium oxide will not change remarkably. The same effect is observed for ion-beam oxidation of silicon targets, where the reaction constants at 1 and 5 keV are so large that they lead to 100% oxidation in both cases.

This can be more clearly seen in Fig. 13 where we show the mean degree of oxidation, calculated with CISRD, as a function of the reaction constant. These data have been calculated using the different values of the reaction constant for a simplified matrix of pure Ga, As, or Si, since we wanted to emphasize the variation of relative degree of oxidation with the energy. The As degree of oxidation changes over a factor of 5.9 from 5 to a 1 keV bombardment. For Ga, this change is only 1.5, while Si exhibits the same degree of oxidation for both reaction constants considered.

B. Depth profile simulation for steady state

The CISRD model applied to the 1 and 5 keV O_2^+ bombardments at normal incidence on GaAs results in the internal profiles shown in Figs. 14 and 15. Note that for both Figs. 14 and 15, the surface of the simulated internal profiles starts at 8.4 and 25.5 nm with respect to the original surface, respectively. These offsets correspond to the amount of material removed by sputtering.

The depth profile for 1 keV bombardment presents an oxide layer of about 5.4 nm thick with a rather sharp interface with the GaAs bulk. The basic component in the oxide layer is Ga_2O_3, although it is not a homogeneous layer. The oxide is divided in three different sublayers. A first sublayer lies on top of the oxide, with a thickness of approximately 1.0 nm and is basically formed by Ga_2O_3 with only some traces of pure Ga, while it shows a depletion of elemental As and As oxide, stressing the importance of chemical preferential sputtering of As_2O_3 in the surface region. The next sublayer extends over about 1.0 nm below the surface region and contains Ga_2O_3 as the dominant compound plus some pure arsenic. This, likely, results from the fact that the sur-
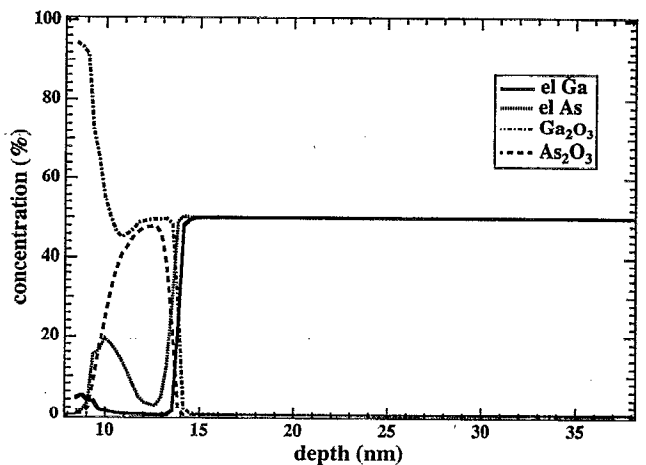
face region (Ga_2O_3) results from As preferential sputtering, while the low $K_{As_2O_3}$ avoids total oxidation. The third sublayer which extends towards the interface with the bulk is a mixture of Ga_2O_3 and As_2O_3. Although the oxidation of arsenic has a very low reaction constant, the accumulation of oxygen in the subsurface region, which is not affected by any desorption, enables the oxidation of As in this region after Ga has become totally oxidized. Table I shows a comparison between the XPS concentrations predicted by the CISRD profile and the in situ XPS measurements (± 3 at. %). A very good agreement is found for both the total concentrations and the partial concentrations of the respective chemical states for each target species.

The structure of the oxide layer formed with a 5 keV O_2^+ ion beam at normal incidence is quite similar to the previous
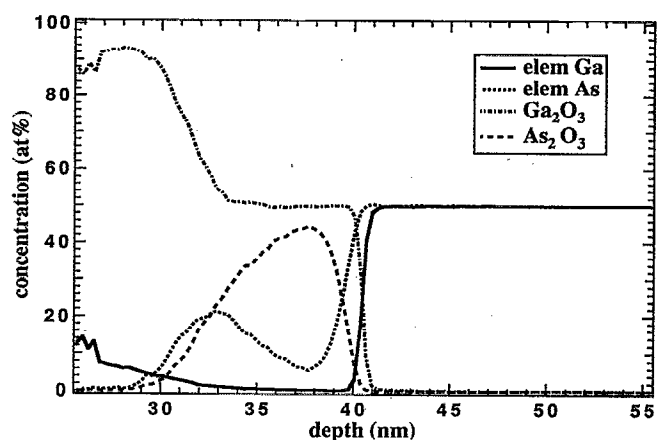

FIG. 15. Steady state internal profile of GaAs after a 5 keV O_2^+ bombardment at normal incidence, simulated using the CISRD model. The depth scale is measured with respect to the original surface, whereas the instantaneous surface is located at the depth of 25.5 nm.

TABLE I. Comparison of XPS atomic concentrations derived from simulation (CISRD) and direct XPS experiment (1 keV O_2^+ bombardment at normal incidence of GaAs).

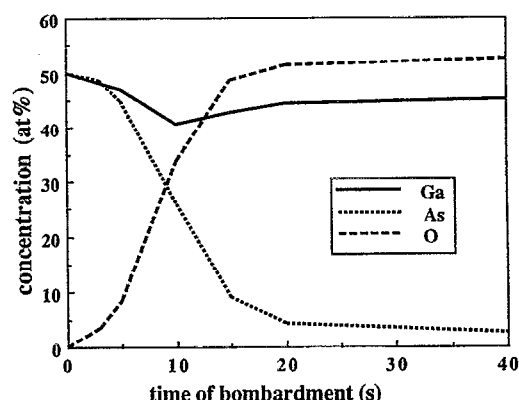|	CISRD XPS (at. %)	Experimental XPS (at. %)
el. Ga	3.3	6.6
el. As	6.5	3.6
Ga(-O)	30.3	28.1
As(-O)	9.1	9.5
Ga	33.6	34.7
As	15.6	13.1
O	50.8	52.2

FIG. 16. CISRD time profile of the total concentrations of Ga, As, and O for a 5 keV O_2^+ bombardment at normal incidence of a GaAs target.

case, although the depletion of arsenic is now more evident. The total thickness of the layer is 14.4 nm, in good agreement with the thickness measured by HREM (14.1 nm). The sublayer structure previously found remains exactly the same, but the respective thicknesses are enlarged (by about a factor of 3). Because of the overall thicker oxide layer the chemical preferential sputtering of As_2O_3 and the subsequent depletion of As become much stronger than for the 1 keV bombardment.

Further the GaAs sputter yield found in the present simulation and defined as the number of sputtered GaAs molecules per incoming ion gives a value of 0.8, which approximates very well the experimental value[22] of 0.85, and supports the validity of the binding and surface binding energies derived in the simulation for Ga, As, Ga_2O_3, and As_2O_3.

The comparison between XPS concentrations of total and fractional chemical states is presented in Table II. The strong tendency to reduce drastically the arsenic oxidation and the increase in gallium oxidation is fully reproduced by the CISRD simulation.

For both simulated depth profiles, the elemental concentrations show some minor discrepancies which are probably related to some uncertainties in the XPS fitting procedure.

C. Dynamic profile

The evolution of the Ga, As, and O species as a function of the time of bombardment (or dose) has been simulated by the CISRD code until the steady state is reached for the case of 5 keV and normal incidence bombardment. In Figs. 16 and 18, the corresponding equivalent XPS concentrations calculated using the Laplace transform are plotted as a func-

tion of the bombardment time. A good agreement is found with the experimental XPS concentrations plotted as a function of the reduced time (RT), which is the ratio between the time of bombardment and the time necessary to reach the steady state (Figs. 17 and 19). It should be noted, however, that the initial sputtering of the native oxide is avoided in the simulations, since the starting target surface (and the bulk) is considered to be a stoichiometric GaAs (1:1), whereas the measured as-received target has a native oxide on top. Once the removal of the native oxide is finished ($0 < RT < 0.06$ in the experimental XPS profile) the CISRD-calculated profile simulates closely the quasiconstant evolution of the total Ga concentration, the strong preferential removal of the total As, and the incorporation of oxygen in the target, in agreement with experiment. The simultaneous decrease of elemental Ga and elemental As while the gallium oxide is growing can also be observed in the simulated time profile as well as the retarded oxidation of As with respect to Ga.

Figure 20 presents the simulated time evolutions of the altered layer depth profile on the GaAs target.

During the early stages of the bombardment ($t < 7$ s) a distortion of the Ga and As concentration levels occurs with an initial consumption of elemental Ga, which reacts with the incorporated oxygen and forms an initial oxide phase all
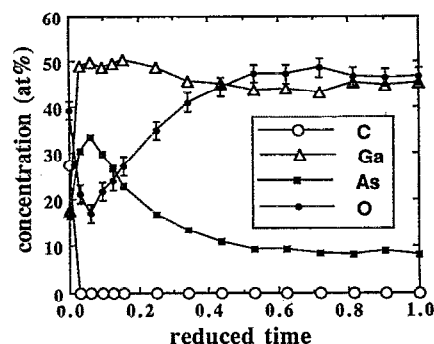
TABLE II. Comparison of XPS atomic concentrations derived from simulation (CISRD) and direct XPS experiment (5 keV O_2^+ bombardment at normal incidence of GaAs).

	CISRD XPS (at. %)	Experimental XPS (at. %)
el. Ga	3.9	7.2
el. As	1.4	6.4
Ga(-O)	41.1	37.9
As(-O)	1.2	1.7
Ga	45.0	45.1
As	2.6	8.1
O	52.3	46.7

FIG. 17. XPS profile of the total concentrations of Ga, As, and O during O_2^+ bombardment of GaAs (5 keV and normal incidence) as a function of reduced time (described in text).
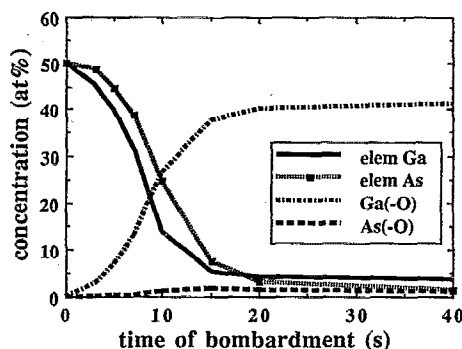
Alay, Vandervorst, and Bender

FIG. 18. CISRD time profile of the total oxidized Ga and As concentrations and elemental Ga and As concentrations for a 5 keV O_2^+ bombardment at normal incidence of a GaAs target.

along the disturbed depth, whereas the As oxidation is a much smaller and slower process.

The Ga oxide continues to grow at a high rate until $t=15$ s, where the rate decreases and a remarkable sharpening of its interface with the bulk is observed, while its oxidation level does not vary significantly. When the Ga oxidation approaches its maximum level close to the interface with the bulk, the As oxidation starts in the same region, although the process is inhibited at the surface region due to the high preferential sputtering of As from the As_2O_3 phase. This As leaves the surface, thus depleting the altered layer in both elemental As and As_2O_3. As a result the oxide layer formed is primarily a Ga oxide superposed on a buried As oxide layer. It is also interesting to see the continuing formation of an elemental As layer in the subsurface region.

V. DISCUSSION

The present results indicate that the incorporation of oxygen as a result of ion bombardment of GaAs and $Al_xGa_{1-x}As$ targets cannot be explained with the simple concept of ion retention during sputtering.[5] The latter would imply a steady state oxygen concentration inversely proportional to the sputter yield and the formation of very thin
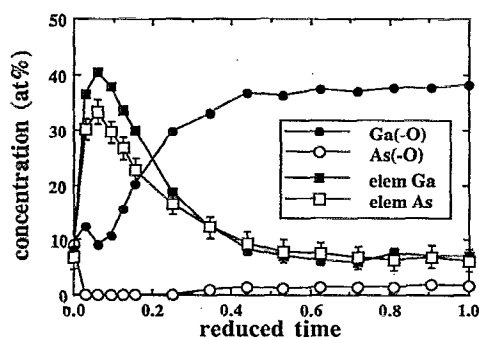

FIG. 19. XPS profile of the total oxidized Ga and As concentrations and elemental Ga and As concentrations during O_2^+ bombardment of GaAs (5 keV and normal incidence O_2^+ bombardment on GaAs).

oxide layers at low energies. In particular, the angular dependence of the oxygen retention provides evidence for an alternative mechanism since the sputter yield is known to vary quite strongly with the angle of incidence and very little variation is found for the oxygen concentration. The thickness of the oxide layers (according to the CISRD simulation and HREM experimental measurements) formed in the O_2^+ range of energies from 1 to 5 keV and normal incidence, is also much larger than would be expected based on the projected range of the primary ions (2–7 nm) for all targets. Both observations indicate that additional effects are contributing to the oxygen retention. Based on the CISRD model for the ion-beam oxidation of GaAs, the diffusion mechanism is responsible for the large oxide thicknesses. The diffusion of the oxygen interstitials incorporated in the oxide layer is the main cause for the reaction of the oxygen atoms with additional target atoms at the interface. Note that this will lead to a thicker layer than expected from the mean projected range for the incoming ions. The diffusion is governed by thermal as well as radiation-enhanced diffusion processes. The latter will be dominant in those regions where point defects (interstitials and vacancies) are created. An additional effect of the radiation-enhanced diffusion is to bring atoms towards the target surface, where they can desorb. As we have shown in the previous sections the oxide thicknesses based on this model (CISRD) agree with the experimental observations (HREM).

The same model can be applied to the $Al_xGa_{1-x}As$ targets (with $x \neq 0$), although the process becomes more complicated because of the presence of aluminum. No detailed modeling of this case has been attempted yet with CISRD. Together with the above described diffusion, surface segregation drives Al and O atoms towards the surface region of the sample (about 5 nm) where they react with oxygen to form the aluminum oxide enriched layer. The HREM observations confirm this model, where a thin aluminum oxide enriched overlayer on top of the altered layer is found, in agreement with recent investigations on the same mechanism during thermal oxidation of $Al_xGa_{1-x}As$ samples.[23] The effect becomes more evident when the Al content increases in the target. The Al migration results in an Al-depleted subsurface layer basically composed of gallium and arsenic oxides. The implementation of this Al segregation will require an additional effort in developing the CISRD program further.

Further ARXPS studies performed on O_2^+ bombarded $Al_{0.4}Ga_{0.6}As$ show that no significant variation is found between small and large takeoff angles for the atomic concentrations, indicating that a rather thick aluminum oxide layer is formed. The oxygen segregation mechanism is necessary to understand the fast oxidation of the aluminum because without such a mechanism, not enough oxygen would be available in the near-surface region to explain the observed Al oxidation. An important conclusion, therefore, from the present work is that the simple retention model is not entirely applicable to GaAs and $Al_xGa_{1-x}As$ targets.

Other differences with the Si case are of course the effects of preferential sputtering in these multielement targets. In GaAs and $Al_xGa_{1-x}As$ we observe a strong preferential sputtering of the As as compared to Ga and Al. This effect is
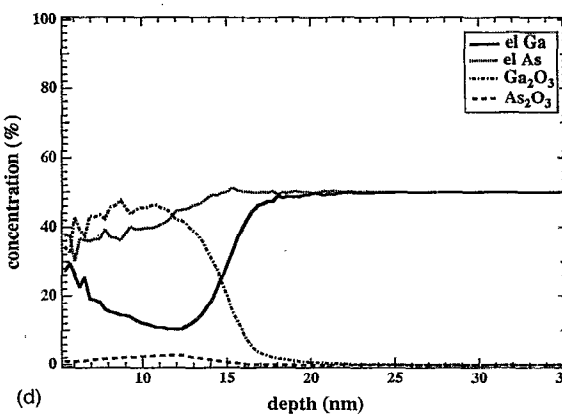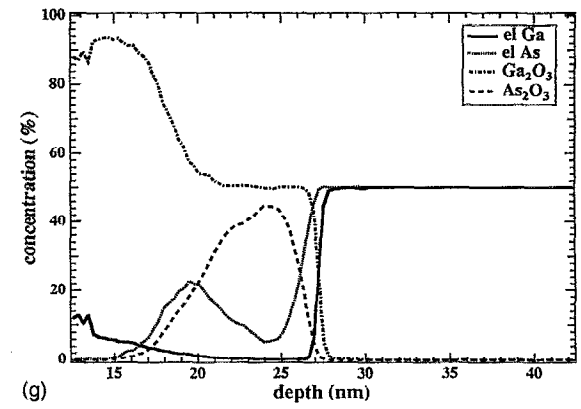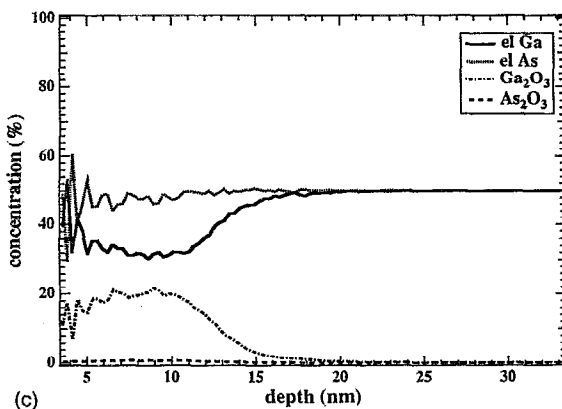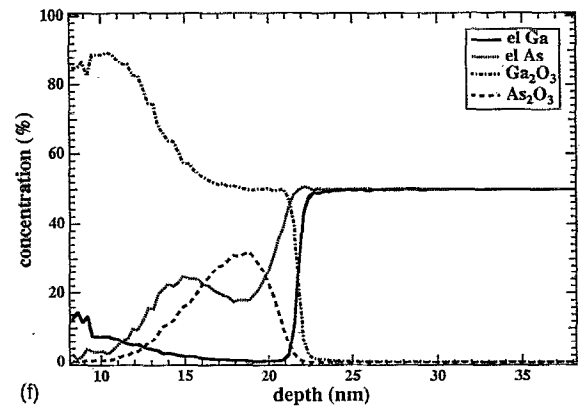
J. Appl. Phys., Vol. 77, No. 7, 1 April 1995

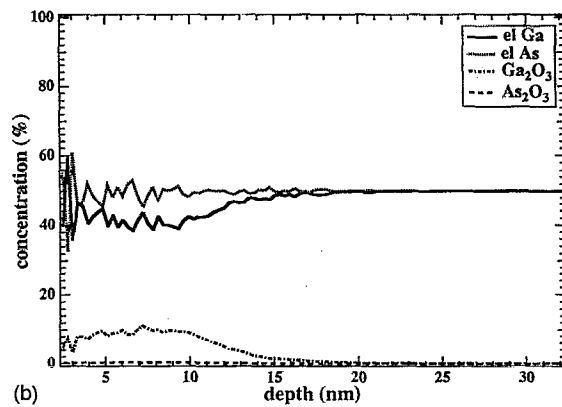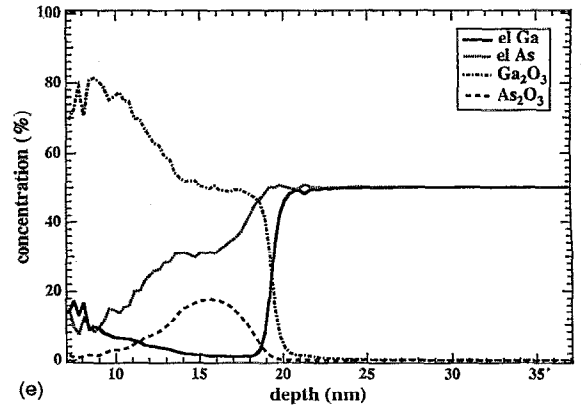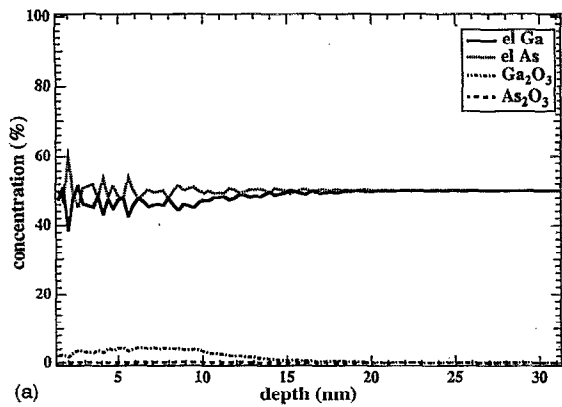Alay, Vandervorst, and Bender   3019

FIG. 20. Depth profiles of GaAs target after a 5 keV O_2^+ bombardment at normal incidence during (a) 3 s, (b) 5 s, (c) 7 s, (d) 10 s, (e) 15 s, (f) 20 s, and (g) 40 s, simulated by the CISRD model.

somewhat reduced at high angles of incidence, indicating that there exists a correlation between the formation of As_2O_3 and preferential sputtering of As; once As_2O_3 is formed, As becomes almost instantaneously sputtered from the surface in a preferential removal mechanism. This can be considered as chemical preferential sputtering (as a consequence of the very low sublimation energy and surface binding energy for this compound).

In GaAs as well as in $Al_xGa_{1-x}As$ a strong energy and angular dependence is found in the oxidation degree of the As, whereas the oxidation degree of Ga and Al seems to be very little influenced. This effect can be explained by thermodynamic considerations, although other processes such as chemical preferential sputtering of the arsenic oxide can also modify the degree of oxidation. It is clear that a competition between Ga and As for the incorporated oxygen takes place when only a limited supply of oxygen is available. Since, for GaAs, the formation enthalpy of the gallium oxide per metallic atom $[\Delta H_f(Ga_2O_3) = -5.54$ eV/metal atom$]$ is lower than the one for the arsenic oxide $[\Delta H_f(As_2O_3) = -3.38$ eV/metal atom$]$, it is expected that Ga will be predominantly oxidized. It is, however, not true that a complete oxidation of Ga is required before As becomes oxidized, although one does observe some delay in the onset of the As oxidation with respect to gallium—a common feature for bombardments on GaAs. This can be explained by the lower enthalpy of formation and consequently by a much lower reaction constant as it was derived in the CISRD simulation.

In the case of $Al_xGa_{1-x}As$ targets, initially, a very rapid oxidation of Al takes place up to 100 rel%. After this oxidation of aluminum, an enhancement of the oxidation of Ga and As occurs in the $Al_xGa_{1-x}As$ samples. The velocity and degree of oxidation cannot be explained only by the large value of the enthalpy of formation for an aluminum oxide $[\Delta H_f(Al_2O_3) = -8.78$ eV/metal atom$]$ which is comparable to that for the formation of silicon oxide $[\Delta H_f(SiO_2) = -9.05$ eV/metal atom$]$. The velocities of Ga and As oxidation found for all targets show a nearly linear relation with the respective heat of formation, while the velocity of Al oxidation does not fit into this dependence especially for high Al content targets. This can be explained in terms of enhanced induced segregation of Al and O towards the surface.

The oxide layer contains, for some bombardments, some elemental components, namely pure Ga and pure As, in a 1:1 ratio, suggesting the possibility of reformation of Ga—As bonds during irradiation. In the HREM micrographs, however, no sizable microcrystalline clusters are seen in the amorphous oxide layer. From the phase diagrams derived for GaAs and its oxides,[24] it is deduced that GaAs is not stable in the presence of As_2O_3. It is, therefore, more likely to have pure As and pure Ga phases coexisting with the respective oxides and aluminum oxide in the case of $Al_xGa_{1-x}As$.

A final important feature is the presence of a thick damaged layer beneath the oxide, as observed by HREM. This layer can be thicker than 15 nm, resulting in an altered layer of approximately 34 nm, far beyond the expected diffusion lengths (18 nm) for the oxygen ions. It was suggested in an
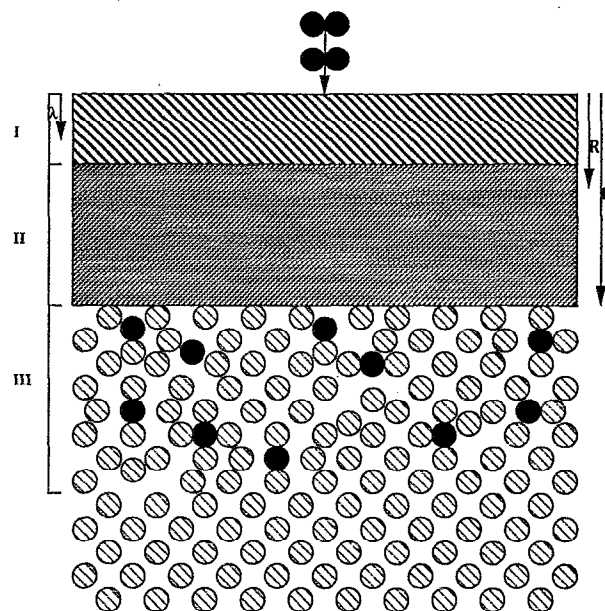

FIG. 21. Schematic of the altered layer (I+II+III) formed by ion-beam induced oxidation of (100) $Al_xGa_{1-x}As$ targets. The light grey top layer represents an Al-oxide enriched layer (I), the dark grey layer a combined Ga, As, and Al oxide (II). The damaged layer (III) and the substrate is represented by an ordered zinc-blende-like lattice. Some oxygen atoms (in black) reside in the damaged region. λ represents the photoelectron attenuation length, R the mean projected range for the incoming ions, and D the diffusion length of O ions.

investigation of ion-beam oxidation carried out on Si, that the long range mobility of the oxygen ions was due to an electric-field enhanced diffusion[25] produced by an electric field of about 10^5 V cm^{-1} across the altered layer. The electric field originated from the constant flow of secondary electrons during the bombardment.

Instead, we find it more plausible to consider the penetration of a small fraction of energetic oxygen ions over rather large ranges as the origin of the damaged layer. This has been tested by using the crystalline-TRIM simulation[26] program, which considers the target as a crystalline zincblende structure. Initially, the aim of this additional simulation was to study the possibility of effective oxygen ion channeling beyond the altered layer in the substrate. The effect turned out to be completely negligible due to the large thickness of the amorphous altered layer. However, the simulation showed the existence of an exponential tail for the concentration of the implanted atoms extending beyond the depth corresponding to the interface oxide substrate. This small tail is considered to be responsible for the substrate damage, observed in the HREM micrographs.

The structure of the altered layer is shown in a schematic way in Fig. 21, which summarizes the various physical mechanisms operative during ion beam induced oxidation. The cross section of the altered layer can be divided into three different regions. Amorphous Al oxide is the dominant

J. Appl. Phys., Vol. 77, No. 7, 1 April 1995

Alay, Vandervorst, and Bender   3021

compound in layer I (in grey color), whereas amorphous layer II (in dark grey color) is formed by a combination of Ga oxide, As oxide, and some Al oxide. Finally, layer III, although retaining crystalline properties, shows heavy damage induced by small fraction of incoming ions (oxygen atoms as black spheres). Note that in the GaAs case, layer I should be replaced mostly by a Ga oxide layer. The various parameters involved in the growth process and in its consecutive analysis are drawn on the right-hand side of Fig. 21: the main part of the sampling depth, by XPS, is characterized by the photoelectron attenuation length (λ), the mean penetration range for the incoming oxygen ions (R), and the diffusion length for oxygen ions (D).

VI. CONCLUSIONS

The analysis of $Al_xGa_{1-x}As$ targets bombarded with oxygen has revealed the preferential oxidation of Ga as compared to As. This effect increases with increasing the bombardment energy and increasing angle of incidence. It has also been observed that the oxygen bombardment of these samples leads to As depleted surfaces due to the strong chemical preferential sputtering of As oxides. The oxygen concentration measured in the stationary state does not relate to the simple model of ion retention during sputtering but implies additionally, a significant indiffusion of the oxygen during irradiation, probably by radiation-enhanced and thermal diffusion mechanisms. A simulation program (CISRD) has been developed, which adequately describes these processes, and shows good agreement with the experimental data. The oxygen diffusion and the induced diffusion of the aluminum towards the surface leads to a very fast complete oxidation of Al during the initial stages of the bombardment. The difference between the As and Ga oxidation velocity, their stoichiometry and degree of oxidation can be explained based on the heat of formation for the respective oxides and the availability of excess oxygen. With respect to the layer structure, the combined HREM-XPS analysis shows how an Al-oxide enriched layer is formed on top of the altered layer for $Al_xGa_{1-x}As$ targets.

[1] J. L. Alay and W. Vandervorst, Surf. Interface Anal. 19, 313 (1992).
[2] N. Herbots, O. C. Hellman, P. A. Cullen, and O. Vancauwenberghe, in Deposition and Growth: Limits for Microelectronics, edited by G. W. Rubloff, American Vacuum Society Series No. 4 [AIP Conf. Proc. 167, 259 (1988)].
[3] W. Reuter, Nucl. Instrum. Methods B 15, 173 (1986).
[4] N. Herbots, O. Hellman, P. Yeh, X. Wang, and O. Vancauwenberghe, in Low Energy Surface Interactions, edited by J. W. Rabalais (Wiley, Cambridge, 1993), Chap. VIII.
[5] F. Schultz and K. Wittmack, Rad. Eff. 29, 31 (1976).
[6] O. Vancauwenberghe, N. Herbots, H. Mahnoharan, and M. Ahrens, J. Vac. Sci. Technol. A 9, 1035 (1991).
[7] J. L. Alay and W. Vandervorst, J. Vac. Sci. Technol. A 10, 2926 (1992).
[8] J. L. Alay and W. Vandervorst, Beam-Solid Interactions: Fundamentals and Applications, edited by M. Nastasi, L. Harriott, N. Herbots, and R. Averback [Mater. Res. Soc. Symp. Proc. 279, 619 (1993)].
[9] O. Vancauwenberghe, N. Herbots, and O. C. Hellman, J. Vac. Sci. Technol. B 9, 2027 (1991).
[10] O. Vancauwenberghe, N. Herbots, and O. C. Hellman, J. Vac. Sci. Technol. A 10, 713, 1992.
[11] C. D. Wagner, W. M. Riggs, L. E. Davis, J. F. Mulder, and G. E. Muilenberg, Handbook of X-Ray Photoelectron Spectroscopy (Perkin–Elmer, Eden Prairie, MN, 1970).
[12] L. A. DeLouise, J. Appl. Phys. 70, 1718, (1991).
[13] G. P. Schwartz, G. J. Gualtieri, G. W. Kammlott, and B. Schwartz, J. Electrochem. Soc. 126, 1737 (1979).
[14] M. P. Seah and W. A. Dench, Surf. Interface Anal. 1, 2 (1979).
[15] A. Romano, J. Vanhellemont, and H. Bender, 1990 Mater. Res. Soc. Symp. Proc. 199, 167 (1990).
[16] J. P. Biersack and W. Eckstein, Appl. Phys. A 34, 76 (1984).
[17] J. P. Biersack and L. G. Haggmark, Nucl. Instrum. Methods 174, 257 (1980).
[18] J. F. Ziegler, J. P. Biersack, and U. Littmack, The Stopping and Range of Ions in Solids (Pergamon, New York, 1985).
[19] J. A. Van Vechten, in Handbook on Semiconductors, edited by S. P. Keller (North Holland, New York, 1980), Vol. 3.
[20] CRC Handbook of Chemistry and Physics, 64th ed., edited by R. C. Weast, M. J. Astle, and W. H. Beyer (Chemical Rubber, Boca Raton, 1983).
[21] R. Kelly, in Ion Bombardment Modification of Surfaces: Fundamentals and Applications (Elsevier, Amsterdam, 1984).
[22] R. Kelly, Surf. Sci. 90, 280 (1979).
[23] W. Vandervorst and K. Miethe, QSA-7 Conference (U.K.), P65 (1992).
[24] A. Mesarwi and A. Ignatiev, J. Appl. Phys. 71, 1943, (1992).
[25] C. D. Thurmond., G. P. Schwartz, G. W. Kammlott, and B. Schwartz, J. Electrochem. Soc. 127, 1366, (1980).
[26] M. G. Dowsett, E. A. Clark, G. D. Spiller, P. D. Augustus, G. R. Thomas, and R. Webb, UK IT88, 512 (1988).
[27] M. Posselt, Nucl. Instrum. Methods B 80/81 (1993).